Climate
of the Past
Discussions
Open Access
EGU

Effect of nitrogen limitation and soil processes on mid–Holocene greening of the Sahara

Jooyeop Lee[1], Martin Claussen[2,3], Jeongwon Kim[1], Je-Woo Hong[4], In-Sun Song[5], and Jinkyu Hong[1]

[1]Ecosystem-Atmosphere Process Laboratory, Department of Atmospheric Sciences, Yonsei University, Seoul, Korea (Republic of)
[2]Max-Planck-Institut für Meteorologie, Hamburg, Germany
[3]Center for Earth System Research and Sustainability (CEN), Universität Hamburg, Germany
[4]Korea Adaptation Center for Climate Change, Korea Environment Institute, Sejong, Korea (Republic of)
[5]Mathematical Atmospheric Physics Lab, Department of Atmospheric Sciences, Yonsei University, Seoul, Republic of)

Correspondence to: Jinkyu Hong (jhong@yonsei.ac.kr)

Abstract. The so–called Green Sahara (GS), wet and vegetative Sahara region in the mid–Holocene, provides useful information on our climate simulation because it is consequence of complex interaction between biophysical and climatic processes. It is still a challenge to simulate the GS in terms of vegetative extent and precipitation using the current climate models. This study attempts to simulate the Green Sahara by using the state–of–the–art earth system model CESM that incorporates the nitrogen cycle and the soil–albedo–precipitation feedback. Our study focuses on the impact of soil biophysical properties and soil nitrogen on the simulation of the GS. With changes in the Earth's orbit and dust in the mid–Holocene, the model simulates increased precipitation in North Africa, but does not capture the extent of the GS. Further analysis shows that the mid–Holocene greening is simulated better if the amount of soil nitrogen and soil texture are properly modified during the GS period through their influence on photosynthesis and surface albedo and their consequent enhanced albedo– and evapotranspiration–precipitation feedbacks. Our findings suggest that future climate simulation needs to consider consequent changes in soil nitrogen and texture with changes in vegetation cover and density for proper climate simulations.

1. Introduction

Sahara is the largest subtropical desert on Earth, but it was wetter and had more vegetation than today during the mid–Holocene (MH hereafter) (Holmes, 2008). In this Green Sahara (GS hereafter) period, the region was covered with various vegetation, inland rivers and mega–lakes (Pachur and Kröpelin, 1987; Jolly et al., 1998; Schuster et al., 2005; Quade et al., 2018) up to 23° N of North Africa, unlike the current vegetation which only exists in regions below 15° N. The GS was sensitive to climate change with locally rapid transitions from a humid to a more arid state some 8,000 to 5,000 years ago (Shanahan et al., 2015). The GS and its transition to an arid state are the results of complex interactions of the orbital forcing changes with the land–atmosphere interaction, and sea surface temperature (SST) variability (Claussen et al. 2017; Braconnot et al., 2019). Our future

Climate
of the Past
Discussions

climate prediction is made using Earth system models (ESMs), and GS is a good platform to evaluate various feedback processes in ESMs accordingly (Harrison et al., 2015; Pausata et al., 2020). In these respects, the GS period provides unique and useful insights for our climate prediction in a changing climate.

35   Many modeling studies have been tried to simulate the GS and understand the underlying mechanisms correctly. Early studies focused on the impacts of change in the Earth's orbit leading to higher summer solar insolation compared to the present (Kutzbach et al., 1981; Kutzbach and Street-Perrott, 1985). Further studies revealed that the following factors contributed to the amplification of the GS; the ocean–climate feedback (Kutzbach and Liu, 1997; Braconnot et al., 1999), vegetation–climate feedback (Claussen, 1998; Claussen et al., 1999; Claussen et al., 2013; Rachmayani et al., 2015; Groner et al., 2018), soil–

40   climate feedback (Kutzbach et al., 1996; Knorr et al., 2001; Levis et al., 2004; Knorr et al., 2006; Vamborg et al., 2011; Lu et al., 2018), inland water (Coe and Bonan, 1997; Krinner et al., 2012), and dust–climate feedback (Pausata et al., 2016; Gaetani et al., 2017). However, current state–of–the–art climate models still yield diverging results regarding the extent of the GS and the understanding of feedback processes (Claussen et al., 2017).

Recent progress in the development of ESMs made it possible to simulate and to assess the carbon–climate feedbacks.

45   Particularly, with the recent inclusion of the nitrogen cycle in the ESM, global carbon budget has been better captured by its downregulation effect of terrestrial gross primary production (GPP) (Thornton et al., 2007; Castillo et al., 2012; Arora et al., 2020). Furthermore, vegetation in the GS led to more simulated organic matter in soils and therefore affecting hydraulic, thermal, and radiative properties of soil. Lu et al. (2018) concluded that soil texture changes likely played an important role in the GS dynamics, but their study was based on the offline land surface model only with changes in soil hydraulic and thermal

50   properties. Although the biophysical and biogeochemical changes in soil are important factors on the GS simulations, no previous studies investigated the GS in perspective of soil carbon and nitrogen in the framework of the ESMs.

The present study aims at assessing the performance of the Community Earth System Model (CESM), version 1.2 (Hurrell et al., 2013) with interactive carbon–nitrogen cycle and dynamic vegetation parameterizations to simulate the mid–Holocene greening of the Sahara. We focus on the ability of the CESM to simulate a Holocene GS and its associated uncertainties related

55   to soil nitrogen and carbon. This enables us to improve our understanding of the model's simulation ability and the representation of physical processes in the CESM land surface model.

2. Methods

2.1 Model description

The Community Earth System Model (CESM, version 1.2) with the Community Atmosphere Model version 4 (CAM4; Neale

60   et al., 2013) and Community Land Model version 4 (CLM4; Oleson et al., 2010; Lawrence et al., 2011) is employed in this study. The CESM incorporates prognostic carbon–nitrogen (CN) equations and the dynamic vegetation model into the land surface model. This new CN parameterization makes a substantial difference in vegetation simulation by limiting gross primary

Climate
of the Past
Discussions

production (GPP) with soil mineral nitrogen in the climate simulations (Thornton et al., 2007; Castillo et al., 2012; Arora et al., 2020):

65 $$GPP = GPP_p \cdot \left(1 - \frac{CF_{excess}}{GPP_p}\right) \tag{1}$$

where GPPp is the potential GPP from the photosynthesis model and CFexcess is the excess of carbon fluxes (Eq. (1)). Appendix A lists the symbols used in this study. CFexcess is calculated as series of functions with soil nitrogen and carbon (Eq. (2) – (7)):

$$CF_{avail\_alloc} = GPP - MR \tag{2}$$

70 $$N_{plant\_demand} = CF_{avail\_alloc} \cdot \frac{k_{n\_alloc}}{k_{c\_alloc}} - N_{retrans} \tag{3}$$

$$N_{uptake} = \frac{N_{sminn}}{\Delta t} - NF_{immob} \tag{4}$$

$$f_{pg} = \frac{N_{uptake}}{N_{plant\_demand}} \tag{5}$$

$$CF_{alloc} = \left(N_{plant\_demand} \cdot f_{pg} + N_{retrans}\right) \cdot \frac{k_{c\_alloc}}{k_{n\_alloc}} \tag{6}$$

$$CF_{excess} = CF_{avail\_alloc} - CF_{alloc} \tag{7}$$

75 In this procedure, soil mineral nitrogen determines the amount of soil nitrogen absorbed by the vegetation and eventually regulates the first estimate of GPP to the smaller final GPP value (Eq. (1)), indicating the importance of the absolute amount of soil nitrogen and carbon when the nitrogen cycle is considered in the model. It was reported that GPP in CESM version 1 was smaller than other CMIP6 models because of larger nitrogen limitation effect. More details on the CN parameterization in the CLM can be found in Thornton et al. (2002), Thornton et al. (2009), and Kluzek (2012). All the symbols and variables 80 used in this study is listed in Supplement.

The albedo–precipitation feedback has been considered to be one of the important aspects in the land–atmosphere interaction (e.g., Charney, 1975; Cess, 1978; Bonfils et al., 2001; Houldcroft et al., 2009; Levine and Boos, 2017). However, in the CMIP5 (Coupled Model Intercomparison Project 5) MH simulations, surface albedo is irrelevant to soil moisture in most LSMs (e.g., Takata et al., 2003; Zeng, 2005; Houldcroft et al., 2009; Oleson et al, 2010; Watanabe et al., 2010; Vamborg et al., 2011). In 85 the CLM4, surface albedo is, however, parameterized as a function of soil moisture in the calculation of soil background albedo. In this parameterization, soil background albedo decreases with increases in soil moisture of the first soil layer as follows:

$$\alpha_{soil} = \alpha_{sat} + \Delta \leq \alpha_{soil} \tag{8}$$

$$\Delta = (0.11 - 0.40\theta_1) > 0 \tag{9}$$

In addition, the soil texture distribution is classified by sand and clay percentage and soil has 20 color classes from low albedo
90 (color class 20) to high albedo (color class 1).

2.2 Experimental design

For our CESM simulations of the GS, the horizontal resolution is 4°×5° in global scale with 26 vertical levels. The initial land
surface data are made using CLM4 offline simulations for 600 years in the CN accelerated decomposition mode (Thornton
and Rosenbloom, 2005), and then using 1200–year CLM4 simulations with the CNDV (Carbon–Nitrogen–Dynamic–
95 Vegetation) with the atmospheric forcing data of 1948–1972 years based on Qian et al. (2006). The present (i.e., 0K) and MH
(i.e., 8K) simulations are 500–year climate simulations using the pre–industrial and MH conditions, respectively (Table 1).
The MH period is set to 8000 years ago (8K) in this study because 8K period was relatively greener than other periods (Jolly
et al., 1998; Groner et al., 2018).

Additional sensitivity experiments using the MH conditions are conducted with different land states to examine the impacts
100 soil nitrogen, soil texture, and the mega lake on the GS simulation (Table 1). In the 8KCN simulation, soil carbon and nitrogen
are increased, and soil texture change to loam iss added to the 8KCN in the 8KCNS (Fig. 1). Soil carbon and nitrogen are
negligible in the current Sahara. To the best of our knowledge, there is no information on soil organic carbon and nitrogen in
North Africa during the MH. It is reasonable to consider more soil carbon and nitrogen in the GS than in the present–day
Sahara, because of their close coupling with biomass (Brooks, 2003; Wang et al., 2010; Yang et al., 2014). To consider the
105 possibility of relatively larger soil carbon and nitrogen in the GS, initial soil carbon and nitrogen in the vegetated area reported
by Jolly et al. (1998) (i.e., 10–22° N, 345° W–40° E) are prescribed using nearby grassland grid values in the 8KCN (Fig. 1).
In all MH simulations, the Earth's orbital parameters and atmospheric CO_2 concentration are prescribed based on Berger (1978)
(Table 2), and atmospheric dust is reduced following Pausata et al. (2016) (Fig. 2). In addition, the Mega Lake Chad is
considered in our MH simulations by assigning 73% of the two grids near the Lake Chad region (14–18° N, 15° E) as lake
110 area to consider the extensive Lake Chad in the MH (Leblanc et al., 2006; Quade et al., 2018). Our analysis focuses on three
critical regions in North Africa around the border of the vegetation in our simulation: the North Africa of 20° N (solid boxed
area in Fig. 3, NA hereafter), northern Sahara–Sahel region (dotted box area in Fig. 3, NSS hereafter), and Southern Sahara–
Sahel region (dashed box area in Fig. 3, SSS hereafter).

3.1 Climate and vegetation simulation in the Green Sahara

115 Figure 3 shows the differences of surface climates between the 0K and 8K experiments in North Africa (8K-0K). The 8K
simulation shows climate patterns in the Sahara–Sahel (SS) region during the MH. The summer downward radiation at the top
of the atmosphere increases by 6% in the SS region than the present because of the change in the orbital forcing and less
amount of dust in the MH. This increase leads to an increase in surface shortwave radiation and net radiation by 30 and 21 W
m^{-2}, respectively and subsequent temperature warming by 1.8° C in the NA region in the 8K experiment (Fig. 3). This

120   intensified land–sea thermal contrast yield spatial changes in precipitation and wind pattern over Holocene North Africa compared to the present climate.

However, the increase in air temperature is not substantial in the southern part of the NA area, because the increase in precipitation and clouds with the northward migration of the monsoon (Fig. 3d). In the 8K experiment, meridional wind in the 18° N region changed from northerly (– 0.7 ms^{-1}) to southerly (0.3 ms^{-1}) in the MH (Fig. 3g, 3h), indicating a northward shift

125   of the Intertropical Convergence Zone (ITCZ) (i.e., the convergence zone of the trade winds) to above 18° N. This ITCZ shift made a favorable condition for a moister Sahara by transporting more moisture and subsequent more precipitation in both of the NSS and SSS region (Chikira et al., 2006; Larrasoaña et al., 2013). Compared to the pre–industrial simulation (i.e., 0K), summer precipitation in the MH simulation (i.e., 8K) increases by 18% (from 4.0 to 4.7 mm day^{-1}) and 15% (from 2.5 to 2.9 mm day^{-1}) in the SSS and NSS region, respectively (Fig. 3e, 3f).

130   The pre–industrial simulation captures the observed spatial extent of the current Sahara based on MODIS (Moderate Resolution Imaging Spectroradiometer) land surface data (Fig. 4a) (Broxton et al., 2014). However, the model does not simulate increased vegetation fraction, despite the increased precipitation over the SS region during the MH (Fig. 4b). Reconstruction of vegetation based on the pollen records reveals that grass and trees expanded up to 26° N and 20° N over North Africa during the GS period, respectively (Hely et al., 2014; Hopcroft et al., 2017). Also, leaf wax data indicated that the GS extended more

135   up north to 31° N (Tierney et al., 2017). In contrast to proxy data, vegetation fraction and GPP shows negligible changes in North Africa and even a decrease in western Africa and southern border of the current Sahara in the 8K simulation (Fig. 4b, 4e).

Hopcroft et al. (2017) attributed such underestimation of the GS to excessive precipitation requirement for vegetation growth in the model (Table 3). Indeed, our investigation shows that the minimum amount of precipitation for vegetation growth is 577

140   mm year^{-1} in the 8K experiment. Notably, this precipitation threshold for vegetation is larger than the observation value of 281 mm year^{-1} and the values of other land surface models reported in Hopcroft et al. (2017). This larger threshold indicates that our model has relatively little vegetation cover with respect to the same amount of precipitation. However, this uncertainty in the model has not been clearly discussed in previous studies. Our investigation reveals that this excess water requirement by vegetation growth is partially related to soil nitrogen, which is discussed in the next section. It is also notable that Mega–Lake

145   Chad does not make substantial changes in simulated summer precipitation northward movement of the 200 and 412 mm year^{-1} precipitation isohyet for 20 % grassland cover, which is similar to Contoux et al. (2013) (Fig. S1, S2).

3.2 Impact of soil nitrogen on the Green Sahara simulation

The 8KCN experiment is designed to study the effect of an increase in soil nitrogen on the GS. The 8KCN simulation reproduces larger precipitation and vegetative areas with an increase in GPP in the SS region, compared to the 8K experiment

150   (Fig. 4). The precipitation threshold for vegetation decreases to 412 mm year^{-1} in the 8KCN from 577 mm year^{-1} in the 8K experiment (Fig. 5). Consequently, the desert–grassland boundary moves one grid box northward in the 8KCN simulation

compared to the 8K experiment (Fig. 4i). Vegetation fraction increases about twice in the SS region (23 % and 13 % in the SSS and NSS regions, respectively) in the 8KCN experiment. Particularly, the 8KCN experiment shows 3 times larger vegetation fraction than the 8K experiment around the boundary of precipitation changes between the present and MH (about

155   18° N). With this increase in vegetation fraction, the 8KCN experiment shows 3.3 and 5.3 times larger GPP in the NSS and SSS regions, respectively, compared to the 8K experiment (Table 4).

Our analysis shows that this increased vegetation in the 8KCN results from less downregulation due to enhanced soil nitrogen (Eq. (1) and Fig. 6). The nitrogen downregulation fraction defined by GPP/GPPp is about 0.5 and 0.3 in the NSS and SSS regions, respectively, in the 8K experiment and increases about by 0.1 in the SS region in the 8KCN experiment. Also, such

160   an increase in vegetation fraction is approximately proportional to the amount of soil nitrogen and, hence, vegetation fraction increase is substantially smaller in the 8KCNh (i.e., half nitrogen simulation of the 8KCN) compared to the 8KCN (Fig. S3). It is also notable that vegetation types depend on the amount of soil nitrogen, and trees in the 8KCN is substantially replaced by grass and shrub in the simulation with less soil nitrogen (8KCNh).

Further investigation indicates that a weak albedo–precipitation feedback is reinforced with more vegetation in the 8KCN

165   experiment as seen in other studies (e.g., Charney, 1975; Vamborg et al., 2011; Rachmayani et al., 2015). Our results indicate that such feedback reinforcement is found in the 8KCN experiment with an additional 0.1 mm day^{-1} precipitation and expansion of vegetation, especially in the SSS region. In the 8K experiment, the surface albedo decreases compared to the 0K experiment, mainly because of the increase in soil moisture by enhanced precipitation (Fig. 7a and 7b). In the 8KCN simulation, the surface albedo diminishes more, because the vegetation increases more and the surface albedo decreases with increasing vegetation

170   cover.

3.3 Impact of soil texture on the Green Sahara simulation

In the 8K and 8KCN simulations, soil is classified as sandy soil for the present–day Sahara. It is, however, plausible that the soils in the GS were more loamy because of the larger organic matter in soil, which affects porosity, albedo, and hydraulic and thermal properties of the soil (Kutzbach et al., 1996; Levis et al., 2004). Recently, Lu et al. (2018) showed that the

175   simulated greening of the Sahara can be sensitive to changes in soil thermal and hydraulic properties even without soil albedo feedback consideration based on an offline dynamic vegetation modeling of the GS. Our fully coupled ESM simulation of 8KCNS corroborates that soil texture leads to significant changes in vegetation and climate in North Africa due to changes in surface albedo as well as in soil hydraulic and thermal properties.

In our 8KCNS simulation, a change from sandy to loamy soil leads to an increase in soil porosity (i.e., water holding

180   capacity) and to darker soil color. Accordingly, the higher soil moisture and darker soil color reduce the surface albedo altogether in the 8KCNS simulation (see Eq. (9); Fig. 8a, 8b). These changes lead to an increase in net radiation, and more available energy is partitioned into latent heat fluxes (i.e., smaller Bowen ratio), leading to more precipitation in the North Africa (Fig. 8c–8e) through enhanced albedo–precipitation feedback in loamy soils.

Furthermore, it is worth noting that subsequent increases in evapotranspiration amplifies precipitation by moisture recycling
again (e.g., Hopcroft et al., 2017; Groner et al., 2018). Previous studies have shown that the evapotranspiration increase in the
Sahara–Sahel region made an increase in precipitation by weaking the African Easterly Jet (AEJ) (Cook, 1999; Wu et al., 2009;
Rachmayani et al., 2015). Our simulation also reveals that loamy soil and the corresponding vegetation change increases
precipitation with enhanced evapotranspiration and weaker AEJ which is not found in the 8KCN experiment. Our results
suggest that both the nitrogen fertilization and the soil properties are important to simulate the increases in precipitation and
vegetation dynamics. Particularly, such feedback processes are dominant in the western SSS where most of this region is
classified as sandy soil in the ESMs (Fig. 8f–8l). Indeed, vegetation fraction increase was clearly observed especially in the
western SSS (< 10° E) in the 8KCNS experiment, with a 2° N northward movement (15° N to 17° N) of the 20% vegetation
coverage border and its related GPP increases. This result suggests that the western SSS is a hot spot in perspective of soil
texture in the MH simulations.

4. Summary and conclusion

This study aims at exploring the effect of soil nitrogen and soil carbon in an Earth System Model on simulations of the Green
Sahara some 8,000 years ago. As we expected, the northward movement of the tropical rainfall belt and its related precipitation
increases in North Africa are found in the simulations with the 8K conditions and present–day soil nitrogen and soil carbon.
However, despite more precipitation in this region, the meridional extent of vegetation in the Sahara–Sahel transition zone
only marginally differs between the mid–Holocene and present–day simulation, which did not simulate greening in the mid–
Holocene. This inconsistent modeling behavior can be attributed to the unrealistically high threshold of precipitation required
for desert–grassland transition in the terrestrial ecosystem model. We show that this excessive rainfall requirement for
vegetation is lowered, thus making vegetation cover and GPP increases, if we consider enhanced soil nitrogen during the Green
Sahara period. It is also found that in this soil–nitrogen–enhanced simulation, the increase in vegetation cover leads to more
precipitation through the albedo–precipitation. Further sensitivity simulations show that loamy soil having more soil organic
matter also leads to more precipitation and vegetation in the Holocene North Africa through added albedo–precipitation and
evapotranspiration–precipitation feedbacks. Our results indicate that soil nitrogen through downregulation of GPP and
interactive changes in soil texture with vegetation are critical for the Green Sahara simulations. Notably, our findings and their
implications can be extended to the future climate simulations and more attention should be paid to the role of soil
biogeochemical processes in the vegetation dynamics in climate simulations.

Appendices

A. List of symbols and definitions.

Symbols	Definitions
CF_{alloc}	total allocated C flux (gC m^{-2} s^{-1})
CF_{avail_allloc}	C flux available for allocation (gC m^{-2} s^{-1})
CF_{excess}	C flux not allocated due to downregulation (gC m^{-2} s^{-1})
dt	decomposition timestep (seconds)
f_{pg}	fraction of potential GPP (no units)
GPP	gross primary index (gC m^{-2} s^{-1})
k_{c_alloc}	C allocation index
k_{n_alloc}	N allocation index
MR	maintenance respiration (gC m^{-2} s^{-1})
$N_{plant\_ndemand}$	plant N demand (gN m^{-2} s^{-1})
$N_{retrans}$	deployment of retranslocated N (gN m^{-2} s^{-1})
N_{sminn}	soil mineral N (gN m^{-2})
N_{uptake}	plant N uptake (gN m^{-2} s^{-1})
NF_{immob}	Immobilization N flux (gN m^{-2} s^{-1})
α_{sat}	soil background albedo for saturated soil (fraction)
α_{soil}	soil background albedo (fraction)
Δ	variable that depends on the volumetric water content of the first soil layer

Climate
of the Past
Discussions

θ_1	the volumetric soil water content of the first soil layer (m^3 m^{-3})

References

Arora, V. K., Katavouta, A., Williams, R. G., Jones, C. D., Brovkin, V., Friedlingstein, P., Schwinger, J., Bopp, L., Boucher,
O., Cadule, P., Chamberlain, M. A., Christian, J. R., Delire, C., Fisher, R. A., Hajima, T., Ilyina, T., Joetzjer, E., Kawamiya,
220 M., Koven, C. D., Krasting, J. P., Law, R. M., Lawrence, D. M., Lenton, A., Lindsay, K., Pongratz, J., Raddatz, T., Séférian,
R., Tachiiri, K., Tjiputra, J. F., Wiltshire, A., Wu, T., and Ziehn, T.: Carbon–concentration and carbon–climate feedbacks in
CMIP6 models and their comparison to CMIP5 models, Biogeosciences, 17, 4173–4222, https://doi.org/10.5194/bg-17-4173-
2020, 2020.

Berger, A. L.: Long-Term Variations of Caloric Insolation Resulting from the Earth's Orbital Elements 1, Quat. Res., 9, 139–
225 167, 1978.

Bonfils, C., de Noblet-Ducoudre, N., Braconnot, P., and Joussaume, S.: Hot desert albedo and climate change: Mid-Holocene
monsoon in North Africa, J. Climate, 17, 3724–3737, 2001.

Braconnot, P., Joussaume, S., Marti, O., and de Noblet, N.: Synergistic Feedbacks from Ocean and Vegetation on the African
Monsoon Response to Mid-Holocene Insolation, Geophys. Res. Lett., 26, 2481–2484, 1999.

230 Braconnot, P., Zhu, D., Marti, O., and Servonnat, J.: Strengths and challenges for transient Mid- to Late Holocene simulations
with dynamical vegetation, Clim. Past, 15, 997–1024, https://doi.org/10.5194/cp-15-997-2019, 2019.

Brooks, M. L.: Effects of increased soil nitrogen on the dominance of alien annual plants in the Mojave Desert, J. Appl. Ecol.,
40, 344-353, 2003.

Broxton, P. D., Zeng, X., Sulla-Menashe, D., and Troch, P. A.: A global land cover climatology using MODIS data, J. Appl.
235 Meteorol. Clim., 53, 1593–1605, doi:10.1175/JAMC-D-13-0270.1, 2014.

Castillo, C. K. G., Levis, S., and Thornton, P. E.: Evaluation of the New CNDV Option of the Community Land Model: Effects
of Dynamic Vegetation and Interactive Nitrogen on CLM4 Means and Variability, J. Climate, 25, 3702–3714,
doi:10.1175/JCLI-D11-00372.1, 2012.

Cess, R. D.: Biosphere-Albedo Feedback and Climate Modeling, J. Atmos. Sci., 35, 1765–1768, 1978.

240 Charney, J. G.: Dynamics of Deserts and Drought in Sahel, Q. J. Roy. Meteor. Soc., 101, 193–202, 1975.

Chikira, M., Abe-Ouchi, A., and Sumi, A.: General circulation model study on the green Sahara during the mid-Holocene: an

impact of convection originating above boundary layer, J. Geophys. Res., 111, D21103, doi:10.1029/2005JD006398, 2006.

Claussen, M.: On multiple solutions of the atmosphere-vegetation system in present-day climate, Glob. Change Biol., 4, 549–559, 1998.

245 Claussen, M., Kubatzki, C., Brovkin, V., Ganoposki, A., Hoelzmann, P., and Pachur, H. J.: Simulation of an abrupt change in Saharan vegetation in the mid-Holocene, Geophys. Res. Lett., 26, 2037–2040, 1999.

Claussen, M., Bathiany, S., Brovkin, V., and Kleinen, T.: Simulated climate-vegetation interaction in semi-arid regions affected by plant diversity, Nat. Geosci., 6, 954–958, 2013.

Claussen, M., Dallmeyer, A., and Bader, J.: Theory and modeling of the African humid period and the green Sahara, Oxford
250 Research Encyclopedia of Climate Science, https://doi.org/10.1093/acrefore/9780190228620.013.532, 2017.

Coe, M. and Bonan, G.: Feedbacks between climate and surface water in northern Africa during the middle Holocene, J. Geophys. Res., 102, 11087–11101, doi:10.1029/97JD00343, 1997.

Contoux, C., Jost, A., Ramstein, G., Sepulchre, P., Krinner, G., and Schuster, M.: Megalake Chad impact on climate and vegetation during the late Pliocene and the mid-Holocene, Clim. Past, 9, 1417–1430, doi:10.5194/cp-9-1417-2013, 2013.

255 Gaetani, M., Messori, G., Zhang, Q., Flamant, C., and Pausata, F. S. R.: Understanding the Mechanisms behind the Northward Extension of the West African Monsoon during the Mid-Holocene, J. Climate, 30, 7621–7642, https://doi.org/10.1175/JCLI-D-16-0299.1, 2017.

Groner, V. P., Raddatz, T., Reick, C. H., and Claussen, M.: Plant functional diversity affects climate–vegetation interaction, Biogeosciences, 15, 1947–1968, https://doi.org/10.5194/bg-15-1947-2018, 2018.

260 Harrison, S. P., Bartlein, P. J., Izumi, K., Li, G., Annan, J., Hargreaves, J., Braconnot, P. B., and Kageyama, M.: Implications of evaluation of CMIP5 palaeosimulations for climate projections, Nature Climate Change, 5, 735–743, doi:10.1038/nclimate2649, 2015.

Hély, C., Lézine, A.-M., and contributors, A.: Holocene changes in African vegetation: tradeoff between climate and water availability, Clim. Past, 10, 681–686, https://doi.org/10.5194/cp-10-681-2014, 2014.

265 Hopcroft, P. O., Valdes, P. J., Harper, A. B., and Beerling, D. J.: Multi vegetation model evaluation of the Green Sahara climate regime, Geophys. Res. Lett., 44, 6804–6813, 2017.

Hurrell, J. W., Holland, M. M., Gent, P. R., Ghan, S., Kay, J. E., Kushner, P., Lamarque, J.-F., Large, W. G., Lawrence, D., Lindsay, K., Lipscomb, W. H., Long, M. C., Mahowald, N., Marsh, D. R., Neale, R. B., Rasch, P., Vavrus, S., Vertenstein, M., Bader, D., Collins, W. D., Hack, J. J., Kiehl, J., and Marshall, S.: The Community Earth System Model: a framework for
270 collaborative research, B. Am. Meteorol. Soc., 94, 1339–1360, 2013.

Houldcroft, C., Grey, W., Barnsley, M., Taylor, C., Los, S., and North, P.: New Vegetation Albedo Parameters and Global Fields of Soil Background Albedo Derived from MODIS for Use in a Climate Model, J. Hydrometeorol., 10(1), 183–198, 2009.

Jolly, D., Harrison, S. P., Damnati, B., and Bonnefille, R.: Simulated climate and biomes of Africa during the Late Quaternary:
275 comparisons with pollen and lake status data, Quat. Sci. Rev., 17, 629–657, 1998.

Climate
of the Past
Discussions

Kluzek, E.: CESM research tools: CLM4 in CESM1. 0.4 user's guide documentation, National Centers for Atmospheric Research, Boulder, 2012.

Knorr, W., Schnitzler, K. G., and Govaerts, Y.: The role of bright desert regions in shaping North African climate, Geophys. Res. Lett., 28, 3489–3492, 2001.

280   Knorr, W. and Schnitzler, K. G.: Enhanced albedo feedback in North Africa from possible combined vegetation and soil formation processes, Clim. Dynam., 26, 55–63, 2006.

Krinner, G., Lézine, A. M., Braconnot, P., Sepulchre, P., Ramstein, G., Grenier, C., and Gouttevin, I.: A reassessment of lake and wetland feedbacks on the North African Holocene climate, Geophys. Res. Lett., 39, L07701, doi:10.1029/2012GL050992, 2012.

285   Kutzbach, J. E.: Monsoon climate of the early Holocene: Climate experiment with the Earth's orbital parameters for 9000 years ago, Science, 214, 59–61, 1981.

Kutzbach, J. E. and Street-Perrott, F. A.: Milankovitch forcing of fluctuations in the level of tropical lakes from 18 to 0 kyr BP, Nature, 317, 130–134, 1985.

Kutzbach, J., Bonan, G., Foley, J., and Harrison, S.: Vegetation and soil feedbacks on the response of the African monsoon to
290   orbital forcing in the early to middle Holocene, Nature, 384, 623–626, 1996.

Kutzbach, J. E. and Liu, Z.: Response of the African Monsoon to Orbital Forcing and Ocean Feedbacks in the Middle Holocene, Science, 278. 440–443, 1997.

Larrasoana, J. C., Roberts, A. P., and Rohling, E. J.: Dynamics of Green Sahara periods and their role in Hominin evolution, PLoS ONE, 8, e76514, https://doi.org/10.1371/journal.pone.0076514, 2013.

295   Lawrence, D. M., Oleson, K. W., Flanner, M. G., Thorton, P. E., Swenson, S. C., Lawrence, P. J., Zeng, X., Yang, Z.-L., Levis, S., Skaguchi, K., Bonan, G. B., and Slater, A. G.: Parameterization improvements and functional and structural advances in version 4 of the Community Land Model, J. Adv. Model. Earth Sys., 3, 2011MS000045, doi:10.1029/2011ms000045, 2011.

Leblanc, M., Favreau, G., Maley, J., Nazoumou, Y., Leduc, C., Stagnitti, F., van Oevelen, P. J., Delclaux, F., and Lemoalle, J.: Reconstruction of Megalake Chad using Shuttle Radar Topographic Mission data, Palaeogeogr. Palaeocl., 239, 16–27,
300   doi:10.1016/j.palaeo.2006.01.003, 2006.

Levine, X. J., and W. R. Boos: Land surface albedo bias in climate models and its association with tropical rainfall, Geophys. Res. Lett., 44, 6363-6372. 2017.

Levis, B. S., Bonan, G. B., and Bonfils, C.: Soil feedback drives the mid-Holocene North African monsoon northward in fully coupled CCSM2 simulations with a dynamic vegetation model, Clim. Dynam., 23, 791–802, doi:10.1007/s00382-004-0477-
305   y, 2004.

Lu, Z., Miller, P. A., Zhang, Q., Zhang, Q., Wårlind, D., Nieradzik, L., Sjolte, J., and Smith, B.: Dynamic vegetation simulations of the mid-Holocene Green Sahara, Geophys. Res. Lett., 45, 8294-8303, 2018.

Neale, R. B., Richter, J., Park, S., Lauritzen, P. H., Vavrus, S. J., Rasch, P. J., and Zhang, M.: The Mean Climate of the Community Atmosphere Model (CAM4) in Forced SST and Fully Coupled Experiments, J. Climate, 26, 5150–5168,

310   doi:10.1175/JCLID-12-00236.1, 2013.

Oleson, K. W., Lawrence, D. M., Bonan, G. B., Flanner, M. G., Kluzek, E., Lawrence, P. J., Levis, S., Swenson, S. C., Thornton, P. E., Dai, A., Decker, M., Dickinson, R., Feddema, J., Heald, C. L., Hoffman, F., Lamarque, J.-F., Mahowald, N., Niu, G.-Y., Qian, T., Randerson, J., Running, S., Sakaguchi, K., Slater, A., Stockli, R., Wang, A., Yang, Z.-L., Zeng, X., and Zeng, X.: Technical Description of version 4.0 of the Community Land Model (CLM), Tech. Rep. NCAR/TN-478+STR, National Center

315   for Atmospheric Research, Boulder, Colorado, USA, 2010.

Pausata, F. S. R., Messori, G., and Zhang, Q.: Impacts of dust reduction on the northward expansion of the African monsoon during the Green Sahara period, Earth Planet. Sc. Lett., 434, 298–307, 2016.

Pausata, F. S., Gaetani, M., Messori, G., Berg, A., de Souza, D. M., Sage, R. F., and deMenocal, P. B.: The Greening of the Sahara: Past Changes and Future Implications, One Earth, 2, 235–250, 2020.

320   Quade, J., Dente, E., Armon, M., Dor, Y. B., Morin, E., Adam, O., and Enzel, Y.: Megalakes in the Sahara? A review, Quat. Res., 90, 253-275, 2018.

Rachmayani, R., Prange, M., and Schulz, M.: North African vegetation-precipitation feedback in early and mid-Holocene climate simulations with CCSM3-DGVM, Clim. Past, 11, 175–185, doi:10.5194/cp-11-175-2015, 2015.

Schuster, M., Roquin, C., Duringer, P., Brunet, M., Caugy, M., Fontugne, M., Mackaye, H. T., Vignaud, P., and Ghienne, J.

325   F.: Holocene Lake Mega-Chad palaeoshorelines from space, Quatern. Sci. Rev., 24, 1821–1827, 2005.

Shanahan, T. M., McKay, N. P., Hughen, K. A., Overpeck, J. T., Otto-Bliesner, B., Heil, C. W., King, J., Scholz, C. A., and Peck, J.: The time-transgressive termination of the African Humid Period, Nat. Geosci., 8, 140–144, https://doi.org/10.1038/ngeo2329, 2015.

Stringer, L. C., Akhtar-Schuster, M., Marques, M. J., Amiraslani, F., Quatrini, S., and Abraham, E. M.: Combating land

330   degradation and desertification and enhancing food security: Towards integrated solutions, Ann. Arid Zone, 50, 1-23, 2012.

Takata, K., Emori, S., and Watanabe, T.: Development of the minimal advanced treatments of surface interaction and runoff, Global Planet. Change, 38, 209–222, doi:10.1016/S0921- 8181(03)00030-4, 2003.

Thornton, P. E., Law, B. E., Gholz, H. L., Clark, K. L., Falge, E., Ellsworth, D. S., Goldstein, A. H., Monson, R. K., Hollinger, D., Falk, M., Chen, J., and Sparks, J. P.: Modeling and measuring the effects of disturbance history and climate on carbon and

335   water budgets in evergreen needleleaf forests, Agr. Forest Meteorol., 113, 185–222, doi:10.1016/S0168-1923(02)00108-9, 2002.

Thornton, P. and Rosenbloom, N.: Ecosystem model spin-up: Estimating steady state conditions in a coupled terrestrial carbon and nitrogen cycle model, Ecol. Model., 189, 25–48, doi:10.1016/j.ecolmodel.2005.04.008, 2005.

Thornton, P. E., Lamarque, J.-F., Rosenbloom, N. A., and Mahowald, N. M.: Influence of carbon-nitrogen cycle coupling on

340   land model response to CO_2 fertilization and climate variability, Global Biogeochem. Cy., 21, doi:10.1029/2006GB002868, 2007.

Thornton, P. E., Doney, S. C., Lindsay, K., Moore, J. K., Mahowald, N., Randerson, J. T., Fung, I., Lamarque, J.-F., Feddema, J. J., and Lee, Y.-H.: Carbon-nitrogen interactions regulate climate-carbon cycle feedbacks: results from an atmosphere-ocean general circulation model, Biogeosciences, 6, 2099–2120, doi:10.5194/bg-6-2099-2009, 2009.

345   Tierney, J. E., Pausata, F. S., and deMenocal, P. B.: Rainfall regimes of the Green Sahara, Sci. Adv., 3, e1601503, https://doi.org/10.1126/sciadv.1601503, 2017.

Vamborg, F. S. E., Brovkin, V., and Claussen, M.: The effect of a dynamic background albedo scheme on Sahel/Sahara precipitation during the mid-Holocene, Clim. Past, 7, 117–131, doi:10.5194/cp-7-117-2011, 2011.

Wang, Y., Li, Y., Ye, X., Chu, Y., and Wang, X.: Profile storage of organic/inorganic carbon in soil: From forest to desert,

350   Sci. Total Environ., 408, 1925–1931, doi:10.1016/j.scitotenv.2010.01.015, 2010.

Watanabe, M., Suzuki, T., O'ishi, R., Komuro, Y., Watanabe, S., Emori, S., Takemura, T., Chikira, M., Ogura, T., Sekiguchi, M., Takata, K., Yamazaki, D., Yokohata, T., Nozawa, T., Hasumi, H., Tatebe, H., and Kimoto, M.: Improved Climate Simulation by MIROC5: Mean States, Variability, and Climate Sensitivity, J. Climate, 23, 6312–6335, doi:10.1175/2010JCLI3679.1, 2010.

355   Wu, M. L. C., Reale, O., Schubert, S. D., Suarez, M. J., Koster, R. D., and Pegion, P. J.: African easterly jet: Structure and maintenance, J. Climate, 22, 4459–4480, https://doi.org/10.1175/2009JCLI2584.1, 2009.

Yang, R., Su, Y., Wang, M., Wang, T., Yang, X., Fan, G., and Wu, T.: Spatial pattern of soil organic carbon in desert grasslands of the diluvial-alluvial plains of northern Qilian Mountains, Journal of Arid Land, 6, 136–144, 2014.

Zeng, X.: Overview of soil, vegetation, and snow albedos in weather and climate models, Annual meeting of the American

360   Meteorological Society, 79, 81-94, 2005.

Table 1: The abbreviations of the numerical experiments conducted in this study.

Abbreviation	Description
0K	500 years simulation using the pre–industrial conditions for orbital forcing and CO_2 concentration (284.725 ppm).
8K	500 years simulation using the mid–Holocene conditions for orbital forcing and CO_2 concentration (Table 2).
8KCN	Same as 8K except that soil carbon and nitrogen are prescribed as the values in the current Sahel region.
8KCN0L	Same as 8KCN except that the Mega Lake Chad is not considered in the simulation.
8KCNh	Same as 8KCN except that soil carbon and nitrogen are prescribed as half of the 8KCN simulation.
8KCNS	Same as 8KCN except that the North African soil was precribed as loam.

365

Table 2: Orbital parameters prescribed for the simulations.

Simulation	CO_2 concentration	Eccentricity	Obliquity	Longitude of Perihelion
0K	284.725 ppm	0.016704	23.44	283.01°
8K, 8KCN, 8KCN0L,8KCNh, 8KCNS	259.9 ppm	0.019101	24.209	148.58°

Climate
of the Past
Discussions

Open Access

EGU

370 Table 3: 20% vegetation coverage transition rainfall for OBS (Observation data) and 4 model simulations (the Joint UK Land Environment Simulator version 4.1, Lund-Potsdam-Jena dynamic vegetation model version 2.1, Sheffield Dynamic Global Vegetation Model, and CLM4 for this study). OBS and JULES, LPJ, SDGVM indicates the value from the observation and model simulation in the pre–industrial conditions which is from Hopcroft et al., 2017.

Model name	20% vegetation coverage transition rainfall (mm yr^{-1})
SDGVM	182
OBS	281
JULES	378
LPJ	515
This study	570 (0K)
	577 (8K)
	412 (8KCN)

375   Table 4: GPP (gC m^{-2} month^{-1}) from 5 CMIP5 models (IPSL-CM5A-LR, MIROC-ESM, bcc-csm1-1, MPI-ESM-P, CCSM4) and this study in NSS region (18–22 °N) during the pre–industrial period (PI) and mid–Holocene (MH).

Model name	PI GPP	MH GPP
IPSL-CM5A-LR	0.00	0.01
MIROC-ESM	0.06	2.69
CCSM4	0.13	0.50
bcc-csm1-1	1.47	1.65
MPI-ESM-P	1.62	5.21
This study	2.12 (0K)	2.27 (8K) 6.79 (8KCN) 6.82 (8KCNS)

17
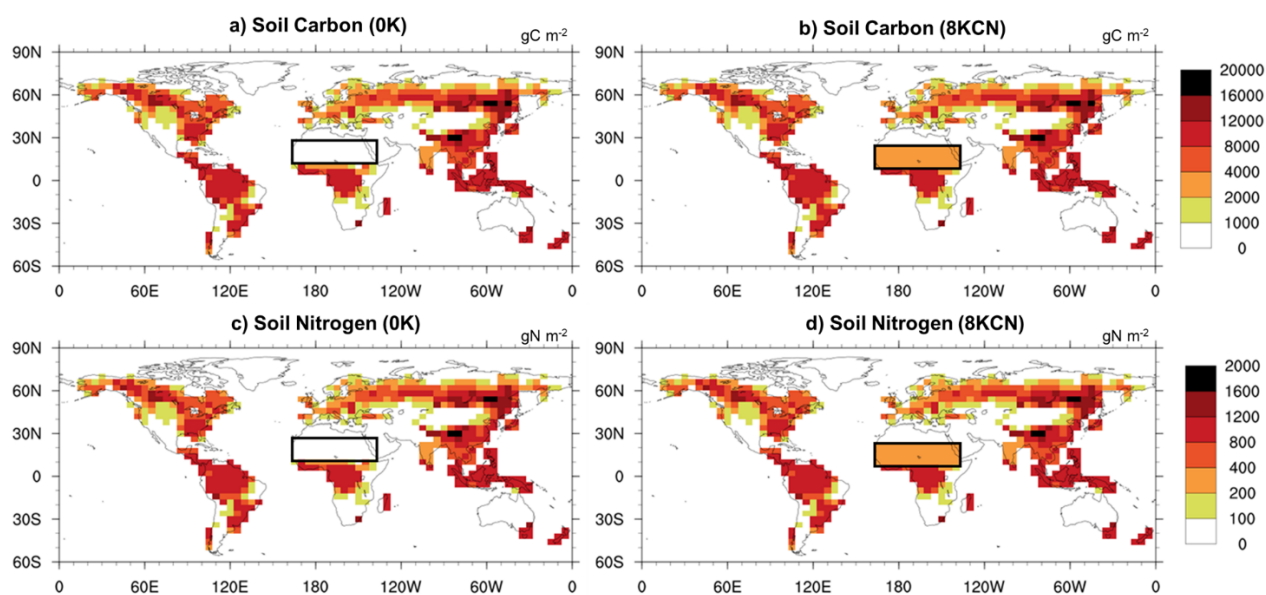
Figure 1: Global maps of soil carbon and nitrogen used in the 0K and 8KCN simulations. Values in boxed area is modified in the 8KCN experiment.
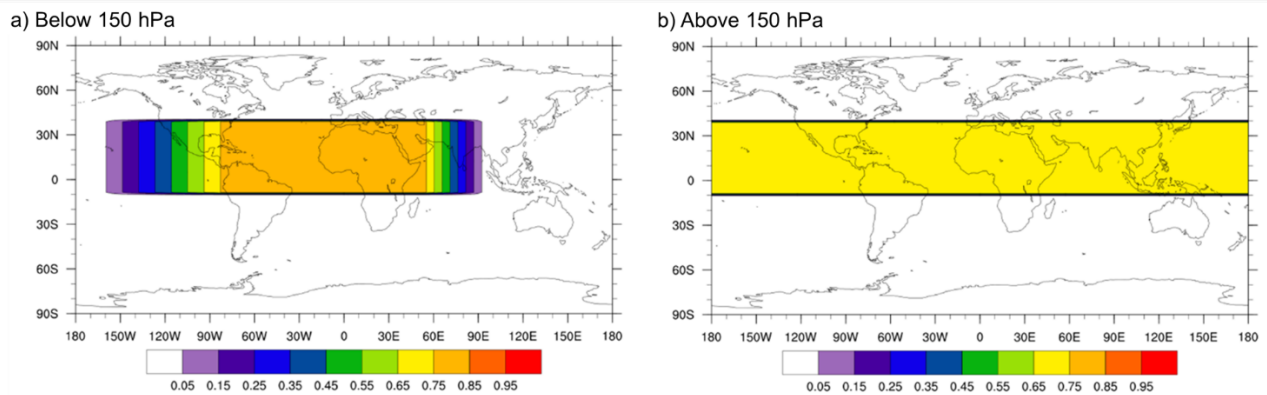
385

Figure 2: Dust reduction fraction a) below 150 hPa and b) above 150 hPa in the mid–Holocene experiments compared to the present–day values.
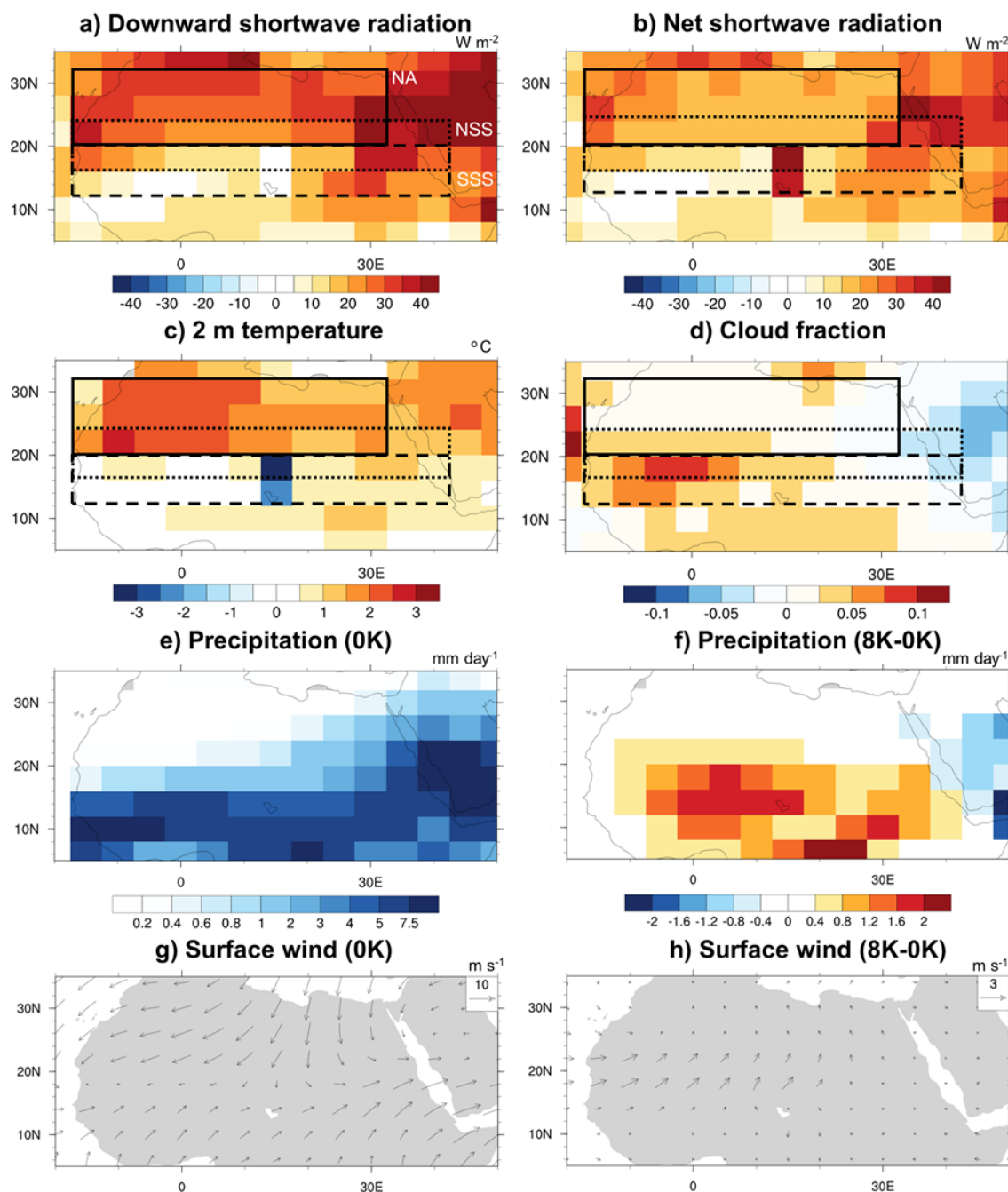
Figure 3: Differences of climate conditions between the 8K and 0K experiment (8K-0K) in summer (June, July, August, and September; JJAS). Differences in downward shortwave radiation (a), surface net shortwave radiation (b), 2 m air temperature (c), and cloud fraction (d). (e) and (f) are JJAS precipitation in the 0K and its differences from the 8K experiment and (g) and (f) JJAS surface wind vector and its differences from the 8K experiment. Black squared boxes are the NA (solid), NSS (dotted), SSS (dashed) areas.
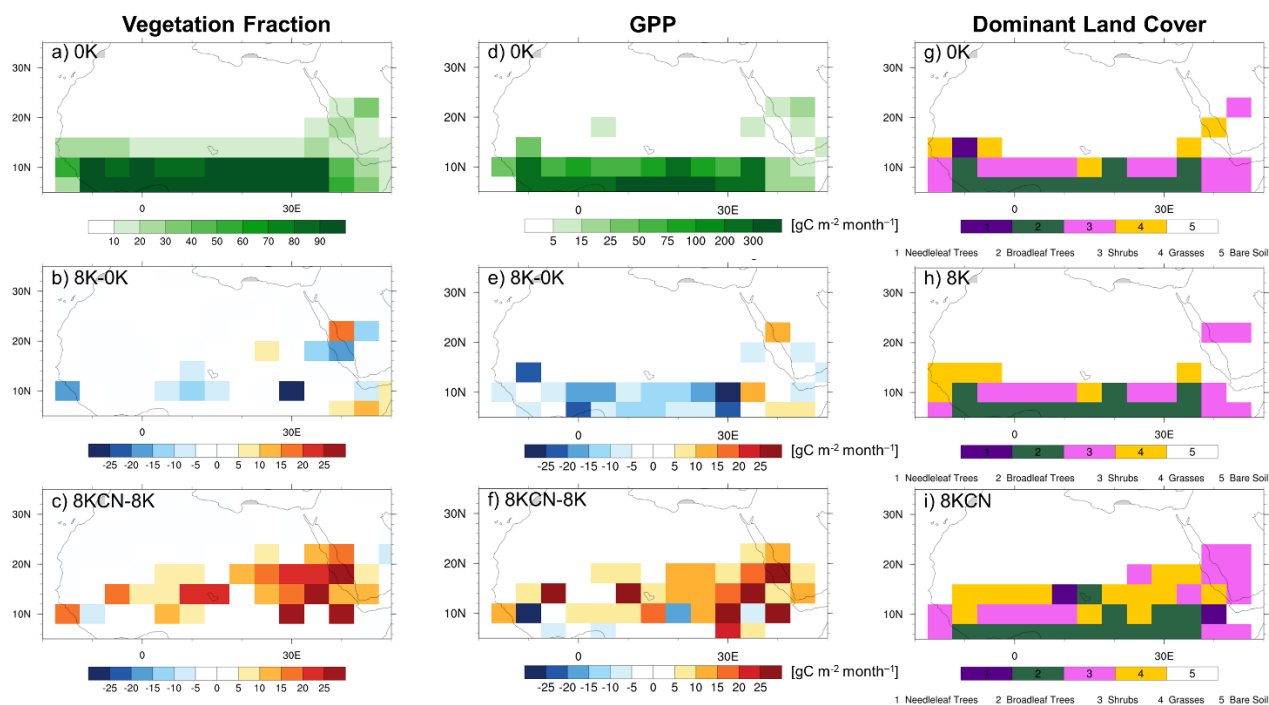
Figure 4: Vegetation fraction (left column), GPP (middle column), and dominant land cover (right column). Panels (b), (e) and (c), (f) are differences between 8K and 0K and between 8KCN and 8K, respectively.
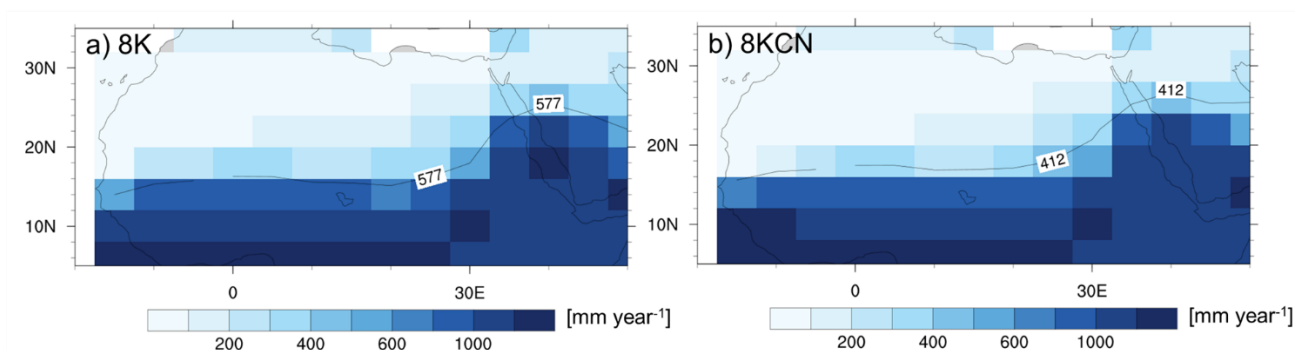
395

400

Figure 5: Annual precipitation in North African from a) the 8K b) 8KCN simulations. The minimum amount of precipitation for vegetation growth boundary is plotted as a black line with its values.
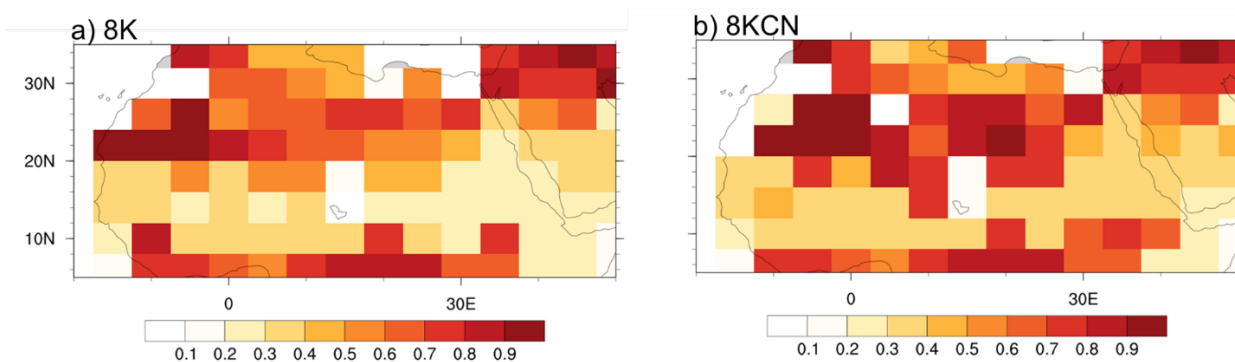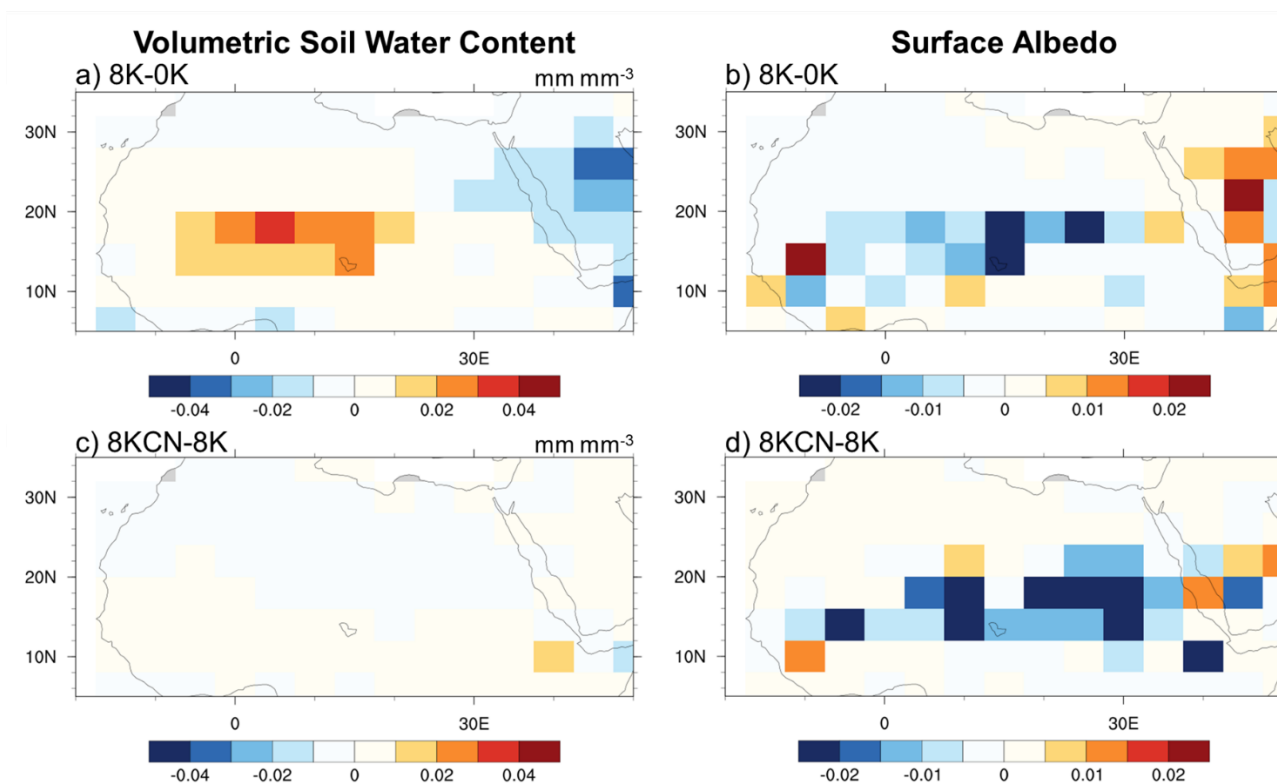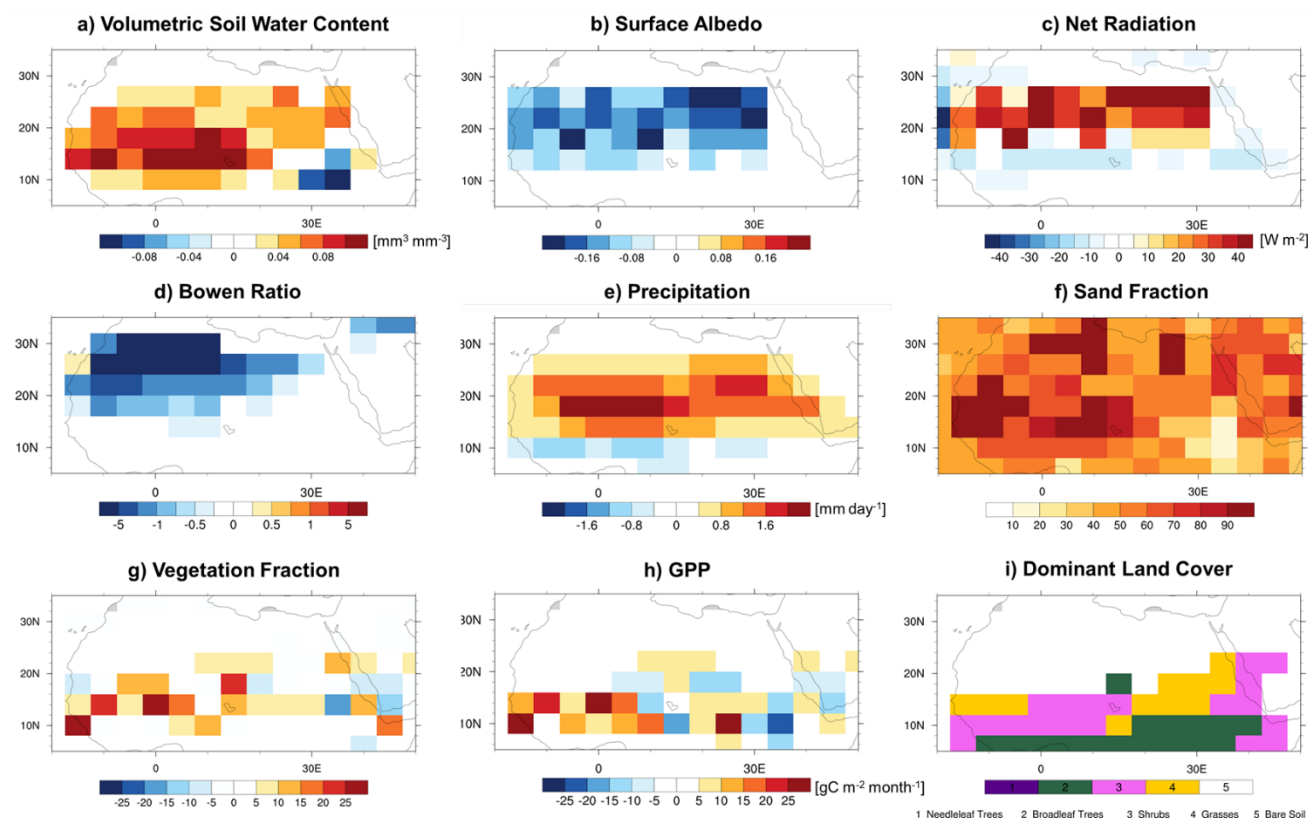
405

Figure 6: Downregulation fraction (GPP divided by GPP not limited by nitrogen) in the a) 8K and b) 8KCN simulations.

Figure 7: Differences in volumetric soil water content (left) and surface albedo (right) between the 0K, 8K, and 8KCN experiments. The first and second rows show the differences between the 8K and 0K, between the 8KCN and 8Kexperiments, respectively.

410

Figure 8: Differences of the loamy soil experiment (8KCNS) from 8KCN. (a) volumetric soil water content, (b) surface albedo, (c) net shortwave radiation, (d) Bowen ratio, (e) precipitation, (f) default sand fraction used in 8K and 8KCN, (g) evapotranspiration, (h) 600 hPa wind of 8KCN, (i) 600 hPa wind difference, (j) vegetation fraction, (k) GPP, and (l) dominant land cover in the 8KCNS experiment.